JACS
JOURNAL OF THE AMERICAN CHEMICAL SOCIETY

Article

pubs.acs.org/JACS

Structural Intermediates during α-Synuclein Fibrillogenesis on Phospholipid Vesicles

Gemma Comellas,[†] Luisel R. Lemkau,[‡] Donghua H. Zhou,[‡,⊥] Julia M. George,[∥] and Chad M. Rienstra*[,†,‡,§]

[†]Center for Biophysics and Computational Biology, [‡]Department of Chemistry, [§]Department of Biochemistry, and [∥]Department of Cell and Developmental Biology, University of Illinois at Urbana−Champaign, Urbana, Illinois 61801, United States

Supporting Information

ABSTRACT: α-Synuclein (AS) fibrils are the main protein component of Lewy bodies, the pathological hallmark of Parkinson's disease and other related disorders. AS forms helices that bind phospholipid membranes with high affinity, but no atomic level data for AS aggregation in the presence of lipids is yet available. Here, we present direct evidence of a conversion from α-helical conformation to β-sheet fibrils in the presence of anionic phospholipid vesicles and direct conversion to β-sheet fibrils in their absence. We have trapped intermediate states throughout the fibril formation pathways to examine the structural changes using solid-state NMR spectroscopy and electron microscopy. The comparison between mature AS fibrils formed in aqueous buffer and those derived in the presence of anionic phospholipids demonstrates no major changes in the overall fibril fold. However, a site-specific comparison of these fibrillar states demonstrates major perturbations in the *N*-terminal domain with a partial disruption of the long β-strand located in the 40s and small perturbations in residues located in the "non-β amyloid component" (NAC) domain. Combining all these results, we propose a model for AS fibrillogenesis in the presence of phospholipid vesicles.

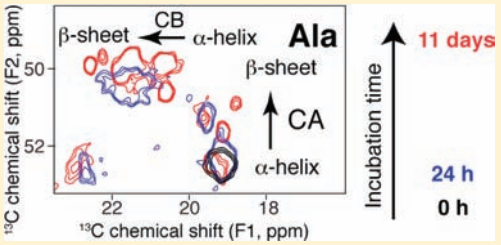

INTRODUCTION

α-Synuclein (AS) is a 14-kDa protein that is unstructured in solution yet forms fibrils that are the primary proteinaceous constituent of Lewy bodies, the pathological hallmark of Parkinson's disease (PD).[1] Three single point mutations (A30P, E46K, and A53T),[2−4] as well as duplication and triplication of the AS allele,[5,6] are associated with familial PD. Despite these substantial associations of AS with disease, the understanding of its folding and misfolding pathways is far from complete. Initial in vitro studies demonstrated that AS binds anionic phospholipids with an increase in α-helical secondary structure.[7,8] Solution NMR studies of AS bound to sodium dodecyl sulfate (SDS) micelles demonstrated that AS residues 3−37 and 45−92 bind via a helical conformation, while the *C*-terminus remains unstructured.[9,10] Recent studies have also reported on binding modes ranging from the free disordered cytosolic form to the anionic phospholipid-bound state[11] and a structure of AS bound to phospholipid vesicles using site-directed spin labeling EPR.[12]

The strong interaction of AS with anionic phospholipids has been shown to promote AS aggregation.[13−17] Smith et al. investigated the transition from α-helical to β-sheet and proposed the formation of an intermediate during fibril formation.[18] Bodner et al. proposed an increased population of a partially disrupted α-helix in the presence of the early-onset PD mutants that may affect the interaction with the membrane bilayer and AS fibrillation.[19] Recent investigations have indicated that AS might form α-helical tetramers that prevent the formation of fibrils.[20] Additionally, changes in the membrane have been detected in the presence of AS protofibrils,[21] with increased effects in the presence of the three mutants.[22] It has also been proposed that the formation of ion channels by AS may destabilize the ionic homeostasis of neurons and cause neuronal cell death.[23−25] Despite all these studies, atomic level structural insights into the aggregation of AS in the presence of lipids are lacking.

Magic-angle spinning (MAS) solid-state nuclear magnetic resonance (NMR) is uniquely able to characterize the structural changes of noncrystalline macromolecules, such as bacteriorhodopsin in the light-driven proton pumping cycle,[26] rhodopsin phosphoactivation,[27,28] and the site-specific investigation of protein folding.[29,30] Previous studies have demonstrated structural analysis of a metastable β-amyloid intermediate in a lyophilized state.[31] Additionally, several groups, including ours, have conducted solid-state NMR studies to investigate the fibrils of AS prepared in aqueous buffer.[32−36] Thus, the application of solid-state NMR is well-suited to provide atomic-resolution structural information of the AS conversion from α-helical to β-sheet fibrils in the presence of physiologically relevant phospholipids. Here we apply this approach to AS fibrils prepared by incubation in the presence of phospholipid vesicles.

Received: September 25, 2011
Published: February 21, 2012

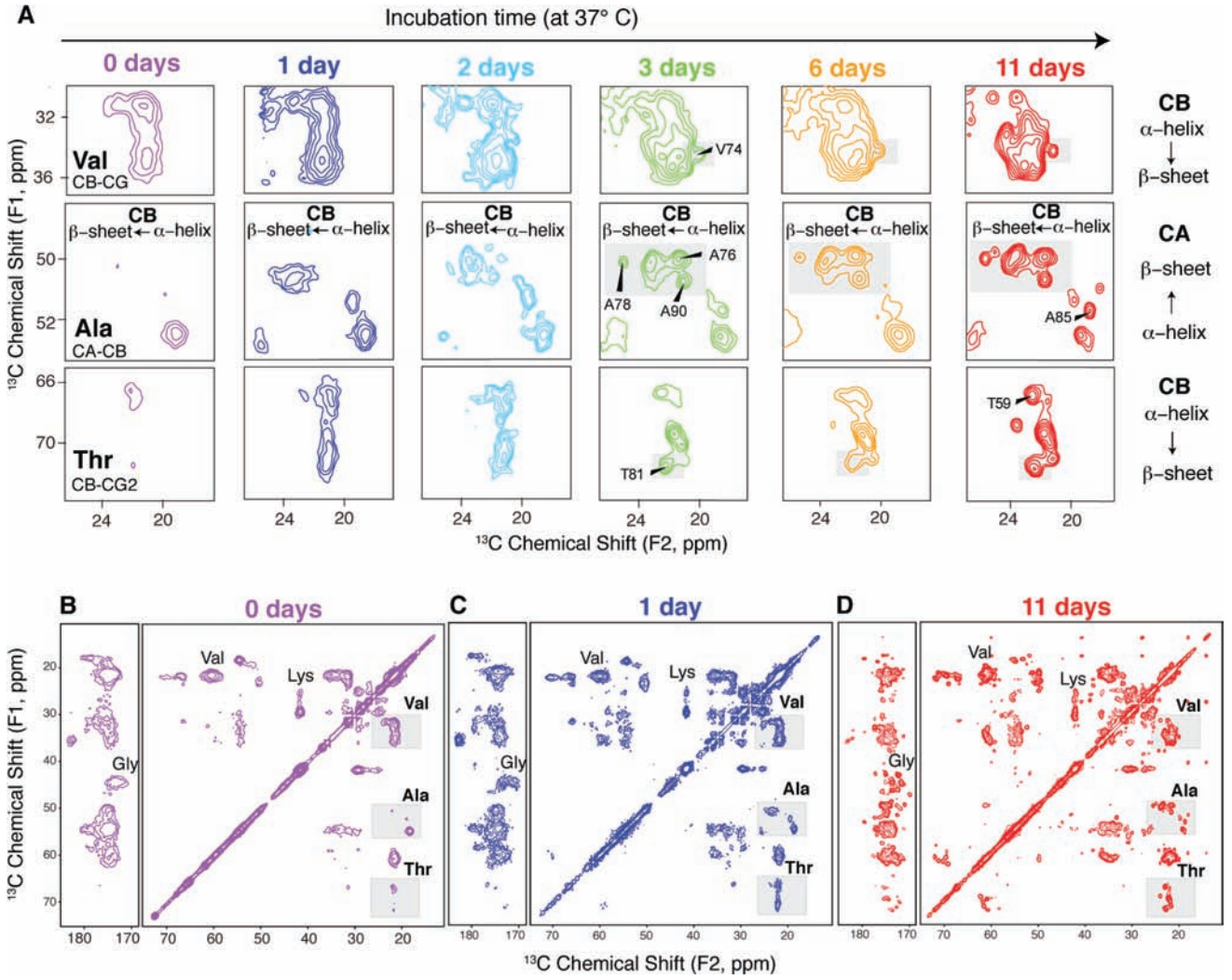

Figure 1. Transition from α-helix to β-sheet evidenced by the changes in chemical shifts of AS incubated in the presence of phospholipid. (A) Expanded regions of $^{13}C-^{13}C$ 2D spectra of AS incubated in the presence of phospholipid for 0, 1, 2, 3, 6, and 11 days. All contours were drawn at ~6σ. Full $^{13}C-^{13}C$ 2D spectra of samples incubated for (B) 0, (C) 1, and (D) 11 days. Expanded regions shown in part A are highlighted in gray.

MATERIALS AND METHODS

Sample Preparation. 1-Palmitoyl 2-oleoyl-*sn*-glycerol-3-phosphatidylcholine (POPC) and 1-palmitoyl-2-oleoyl-*sn*-glycerol-3-phosphate (sodium salt) (POPA) were mixed in chloroform at a 3:1 molar ratio and dried under a stream of N_2. The dry lipids were resuspended in 50 mM sodium phosphate buffer (pH 7.4) with 0.02% NaN_3 and subjected to cycles of freezing–thawing to form vesicles. U-^{13}C,^{15}N-labeled AS was expressed and purified as previously described.[37] AS solutions were prepared at 1 mM concentration in phosphate buffer and passed through a 0.2 μm filter immediately prior to use. AS was added to the lipid solution to reach a lipid-to-protein ratio of 50:1 and an AS concentration of 0.5 mM. The mixture was immediately incubated at 37 °C with shaking (200 rpm) for the defined time of 1, 2, 3, 6, or 11 days under nitrogen atmosphere. At the conclusion of the incubation period, the samples were ultracentrifuged at 110 000*g* for 1 h at 4 °C. Two additional zero time point samples (noted as "0 days incubation") were prepared and ultracentrifuged immediately after adding the AS to the lipid vesicles (and lyophilized directly in the case of the lipid-free sample). In all cases, the pellet from the ultracentrifugation was lyophilized, packed into a MAS rotor and rehydrated, as recently described for fibrils formed in aqueous buffer.[35] Additionally, we measured the approximate lipid-to-protein ratios present in the solid-state NMR rotors based on the integration of the direct-polarization (DP) ^{13}C and ^{31}P 1D spectra versus standard compounds, as described in Table S1 (Supporting Information).

Solid-State NMR Spectroscopy. MAS solid-state NMR experiments were performed using (1) a 11.7 T (500 MHz ^1H frequency) Varian VNMRS spectrometer (Walnut Creek, CA, and Loveland, CO) equipped with a 3.2 mm Varian Balun $^1H-^{13}C-^{15}N$ MAS probe; (2) a 14.1 T (600 MHz, ^1H frequency) Varian Infinity Plus spectrometer with a 3.2 mm HXY narrow bore tuned to double resonance mode for ^1H and ^{13}C frequencies or triple resonance mode for the ^1H, ^{31}P, and ^{13}C frequencies; and (3) a 17.6 T (750 MHz, ^1H frequency) Varian VNMRS spectrometer equipped with a 3.2 mm Varian BioMAS $^1H-^{13}C-^{15}N$ probe (Varian is now part of Agilent Technologies, Santa Clara, CA, and Loveland, CO). All experiments utilized tangent ramped CP.[38] SPINAL-64 ^1H decoupling was applied during acquisition and evolution periods with a field strength of ~75 kHz.[39,40] DARR mixing was used for $^{13}C-^{13}C$ polarization transfer.[41] Chemical shifts were referenced externally with adamantane (assuming the downfield peak at 40.48 ppm).[42]

The majority of $^{13}C-^{13}C$ 2D correlation spectra were acquired at 600 MHz ^1H frequency and 13.3 kHz MAS. Spectra were acquired with 50 ms of DARR mixing,[41] 25.6 ms of acquisition, and 1280 rows of TPPI phase encoded t_1 evolution (dw = 12.5 μs). Spectra were processed with 50 Hz (F1) and 50 Hz (F2) net Lorenzian-to-Gaussian line broadening for all the incubation times, except for some data sets of lower sensitivity, which were processed with 75 Hz (F1) and 75 Hz (F2) net Lorenzian-to-Gaussian line broadening. $^{13}C-^{13}C$ 2D correlation spectra of the 11-day-incubated sample and mature fibrils

dx.doi.org/10.1021/ja209019s | J. Am. Chem. Soc. 2012, 134, 5090–5099

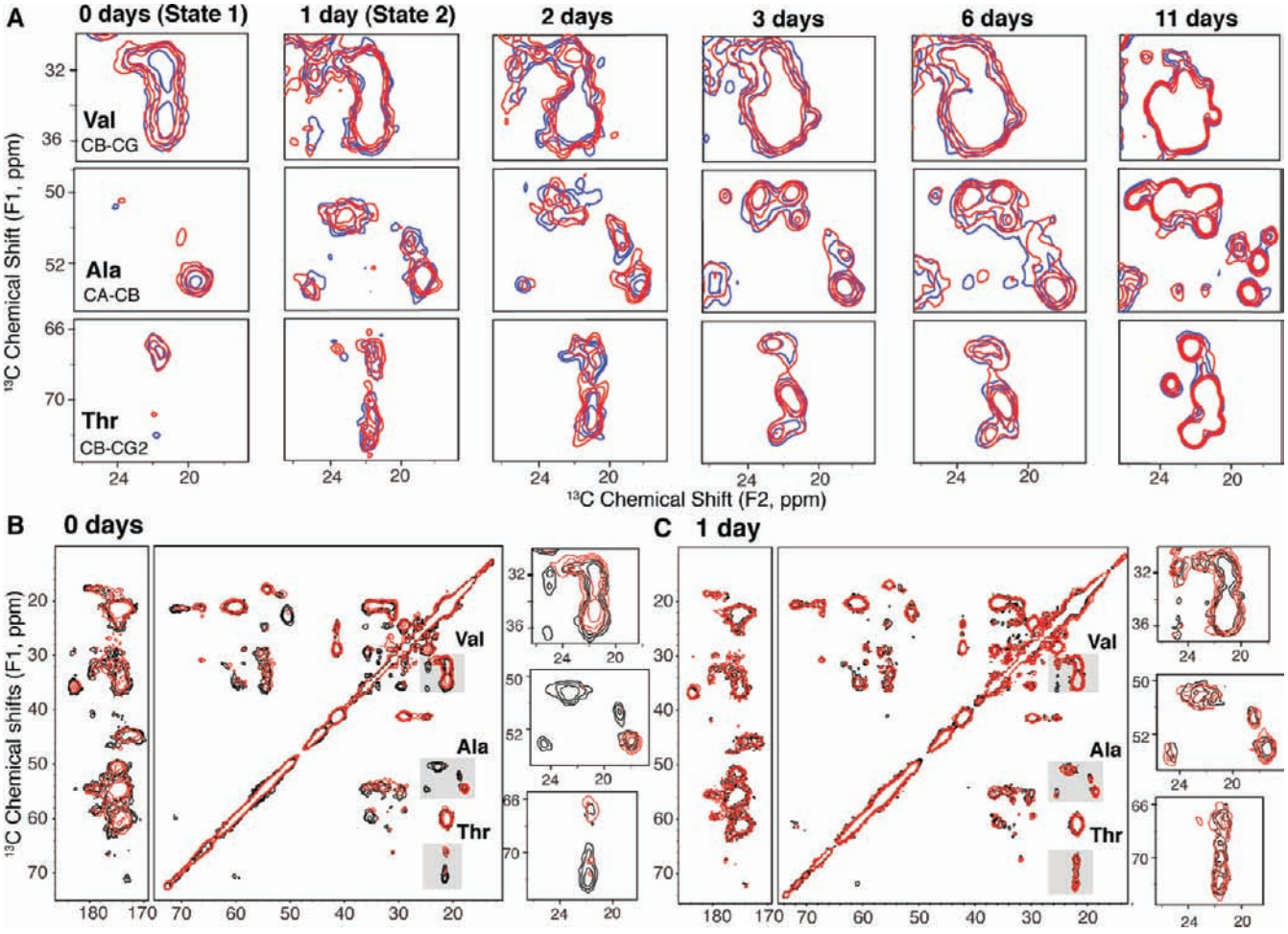

Figure 2. Trapped intermediates are stable during prolonged acquisition of solid-state NMR spectra. U-^{13}C,^{15}N-labeled AS was incubated in the presence of phospholipids for 0, 1, 2, 3, 6, and 11 days. ^{13}C−^{13}C 2D spectra of each sample were acquired over 54 h. (A) Initial (red) and final (blue) 13.5 h blocks overlaid for each time point show that the trapped intermediates were stable during the acquisition of the spectra. Spectra were processed with 75 Hz (F1) and 75 Hz (F2) net Lorenzian-to-Gaussian line broadening. Overlay of the carbonyl and aliphatic spectral regions (with expansions of the Val, Ala, and Thr regions) of two ^{13}C−^{13}C 2D spectra of U-^{13}C,^{15}N-labeled AS incubated in the presence of phospholipids for 0 (B) and 1 days (C). Spectra of the freshly prepared samples are shown in red (with 50 h of total acquisition) and spectra of the same samples 3 months (stored at −20 °C) after preparation are shown in black (30 h of acquisition time). Expanded regions shown in parts B and C are highlighted in gray in the full spectra displayed in parts B and C.

formed in aqueous buffer were acquired on a 750 MHz ^{1}H frequency and 12.5 kHz MAS. Spectra were acquired with 50 ms DARR mixing,[41] 25.6 ms of acquisition, and 768 rows of States-TPPI phase encoded t_1 evolution (dw = 20.0 μs). Spectra were processed with 30 Hz (F1) and 30 Hz (F2) net Lorenzian-to-Gaussian line broadening. All spectra, unless indicated otherwise, were acquired at a variable temperature (VT) of ca. −6 °C, which corresponded to an actual sample temperature of ca. −3 °C, as determined by an ethylene glycol calibration.[43] This is slightly above the phase transition of the lipids in these samples, resulting in optimal resolution and relaxation properties.[44] ^{1}H 1D spectra at VT temperatures from −20 to 10 °C, which correspond to an actual sample temperature from −17 to 13 °C, were acquired to confirm the POPC:POPA (3:1) phospholipid phase transition (Figure S1, Supporting Information). In the gel phase, ^{1}H linewidths decrease and signal intensity increases as the temperature increases. Upon raising temperature through the phase transition and entering the liquid crystal phase, the ^{1}H linewidths decrease dramatically.

2D ^{1}H spin diffusion ^{1}H−^{13}C experiments[9,10] were acquired at 600 MHz ^{1}H frequency, 13.3 kHz MAS, utilizing several ^{1}H−^{1}H mixing times to assess the polarization transfer dynamics. Spectra were acquired with 20.5 ms of acquisition and 256 rows of TPPI phase encoded t_1 evolution (dw = 10.0 μs) and processed with 100 Hz (F1) and 15 Hz (F2) net Lorenzian-to-Gaussian line broadening. ^{1}H spin diffusion ^{1}H−^{13}C spectra were performed with the VT gas adjusted to 10 °C, which corresponds to an actual sample temperature of ∼13 °C, significantly above the lipid phase transition, to enable an efficient T_2 filter for lipid acyl chain ^{1}H signals.

Data Processing and Analysis. All spectra were processed with NMRPipe, with back linear prediction and polynomial baseline correction in the direct dimension. Zero-filling and Lorentzian-to-Gaussian apodization and/or cosine bells were applied for each dimension before Fourier transformation. Peak picking and assignments were performed in Sparky.[45] For quantitative analysis of 2D spin-diffusion spectra, ^{1}H cross sections were extracted from the 2D spectra for the ^{13}C frequencies ranging from 50 to 70 ppm. Peak intensities were plotted as a function of the square root of the ^{1}H−^{1}H mixing time (τ_{mix}) and corrected for T_1 relaxation during the mixing time by multiplication with $\exp(\tau_{mix}/T_1)$.

Electron Micrographs. Samples for electron microscopy were ultracentrifuged and the supernatant and pellets were separated. At this point, both the pellets and supernatant were resuspended in buffer and Karnovsky's fixative was added. Samples were applied to Formvar carbon-coated grids (300 mesh), negatively stained with 2% ammonium molybdate (w/v), and viewed with a Hitachi H600 transmission electron microscope (TEM), operating at 75 kV. To

dx.doi.org/10.1021/ja209019s | J. Am. Chem. Soc. 2012, 134, 5090−5099

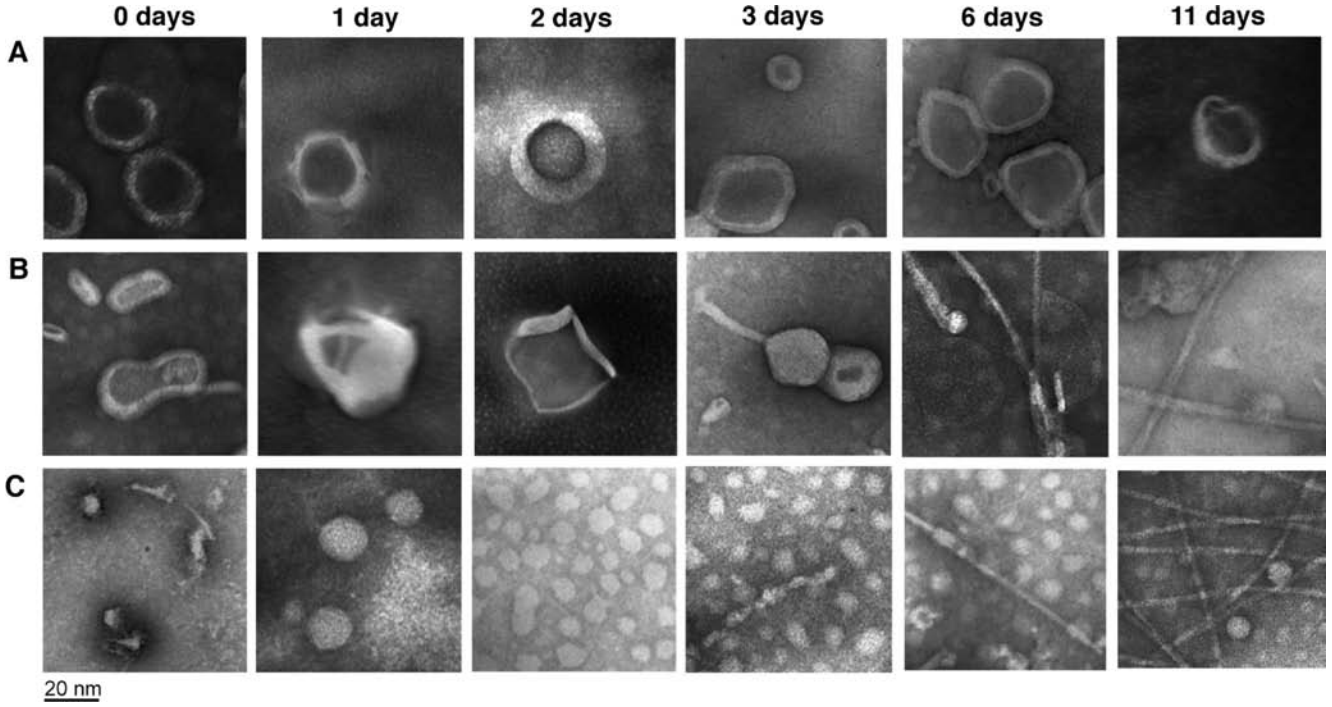

Figure 3. Electron micrographic comparison of samples incubated for 0, 1, 2, 3, 6, and 11 days: (A) phospholipid controls, (B) AS in the presence of phospholipids, and (C) AS in the absence of phopholipids.

ensure uniform vesicles for the microscopy measurements, after evaporating the chloroform from the phospholipids mixture, these were dissolved in buffer and drawn into a Hamilton (Reno, NV) 1 mL gastight syringe. The syringe was placed in an Avanti Polar Lipids Mini-Extruder and the lipid solution was passed through a 0.20 μm Millipore (Billerica, MA) polycarbonate filter 21 times. The newly formed vesicles were collected in the syringe that did not contain the original suspension.

RESULTS AND DISCUSSION

Characterization of the α-Synuclein Fibril Formation Time Course in the Presence of Anionic Phospholipids. In order to structurally characterize the AS fibril formation time course and monitor the transition from a highly α-helical to a β-sheet conformation in the presence of anionic phospholipids, six samples were prepared as described in the Materials and Methods section. These samples were incubated at 37 °C for defined time periods (0, 1, 2, 3, 6, and 11 days) and 2D $^{13}C-^{13}C$ NMR spectra were acquired for each sample under identical instrumental conditions. A comparison of these spectra, emphasizing the Ala, Thr, and Val spectral regions corresponding to the *N*-terminal (residues 1−60) and NAC (residues 61−98) domains (Figure 1A), illustrates that early in the time course AS is predominantly α-helical (state 1), based on secondary chemical shifts resolved by amino acid type. Ala, Thr, and Val residues—all of which are prevalent throughout the *N*-terminal and NAC domains of AS—show exclusively α-helical patterns of shifts, consistent with EPR studies.[12,46,47] After 1 day of incubation, the conversion to β-sheet is evident from the change in chemical shifts of the same spin systems (Figure 1). Further conversion is evident after 3 days of incubation and accompanied by an increase in spectral resolution, an indication of a more homogeneous structure. This structural maturation continues at the 6 day time point, and after 11 days the peak linewidths and most of the spectral fingerprints converge to a state that is predominantly consistent with those of mature fibrils prepared by in vitro incubation in aqueous buffer without lipids.[35]

These results support the following model of AS fibrillogenesis. The *N*-terminus and NAC domain of AS bind to vesicles with an α-helical conformation (state 1), based on the detection of specific residue types only present in this region of the sequence, such as Thr or Val (Figure 1A, 0 days). Next, AS nucleates and converts into a distinct β-sheet secondary structure (Figure 1A, 1 day). Specifically, the $^{13}C-^{13}C$ 2D spectrum of the 1 day sample (state 2) shows patterns of peak intensities that cannot be accounted for by a superposition of the initial and final states. For example, the Thr CB-CG2, Val CB-CG, and Ala CA-CB regions (Figure 1A) show minimal methyl chemical shift dispersion in state 2; the methyls are all within a range of ∼1 ppm. As the sample matures into a well-ordered fibril with long-range order (Figure 1A, ∼3−11 days), packing interactions among side chains lead to a greater dispersion of methyl shifts, in a manner reminiscent of the distinctive methyl shifts of V50 in the HP35 villin headpiece subdomain, which were attributable to tertiary contacts with a ring current effect.[29,48] Side chain packing leads to greater dispersion of methyl ^{13}C shifts, which is what is observed in the mature fibrillar state here.

To ensure that the structural changes only occur during the incubation, not during the course of the NMR measurements, we removed excess monomeric AS at the time of trapping each sample and collected most solid-state NMR data sets at a sample temperature of ca. −3 °C, in comparison to an incubation temperature of 37 °C. For confirmation, we evaluated the initial and final blocks of the $^{13}C-^{13}C$ 2D spectra, which were collected in ∼3−4 h intervals (Figure 2) for a total of ∼50 h. The spectra showed no changes over this time period. We also re-examined the 0, 1, and 11 day samples following several months of storage (at −20 °C, except for periods of NMR data collection). In the case of the 0 h

dx.doi.org/10.1021/ja209019s | J. Am. Chem. Soc. 2012, 134, 5090−5099

incubated sample (state 1), we observed changes in the chemical shifts toward state 2 (Figure 2B); in contrast, the sample incubated for 1 day (state 2) presented unaltered chemical shift patterns for multiple months after the initial data collection, corroborating the trapping of this state (Figure 2C). These results suggest that the conversion of state 2 to mature fibrils might require overcoming a higher energy barrier and/or the presence of additional monomer present in the solution to complete the conversion toward more mature states.

To further investigate AS fibril formation, incubation of AS in the absence of phospholipids was conducted at three different incubation times, 0 h, 1 day, and 3 weeks, to obtain mature fibrils. In contrast to the initial α-helical state observed in the presence of phospholipids, the $^{13}C-^{13}C$ 2D spectra of the 0 h incubated sample demonstrates the presence of initial β-sheet states (Figure S2A, Supporting Information). This result is also supported by the electron micrographs (Figure 3C) with the observation of a few initial oligomer species. Further conversion is evidenced after 1 day, as shown by the changes in chemical shifts in the $^{13}C-^{13}C$ 2D spectra (Figure S2B, Supporting Information). The chemical shifts of this state do not overlap with the initial state or the mature fibrils, suggesting the presence of a new state and not a mixture of the initial and final states. These findings are in agreement with the changes in morphology observed by EM (Figure 3C, 0 and 1 days), from a few small oligomers initially to many particles with well-defined spherical morphology, similar to the intermediate state detected for β-amyloid.[31] Once mature fibrils are formed (Figure 3C), linewidths and chemical shift patterns similar to those of the fibrils formed in the presence of phospholipid vesicles are observed (Figure S2C, Supporting Information).

Further comparison of the two fibrillation pathways was performed by comparing the electron micrographs at different incubation times in the presence and absence of phospholipids, as well as a control experiment with only phospholipids (Figure 3). Once AS is added to the phospholipid vesicles, perturbation of the phospholipid vesicles is apparent (Figure 3A,B, 0 days incubation). After 3 days of incubation, initial linear structures elongating from the vesicles are detected in the presence of AS in comparison to the vesicle controls. These results agree with the solid-state NMR spectra (Figure 1) that exhibit fingerprints of the AS fibril core. Well-defined fibrillar morphologies can be observed after 6 days of incubation, and a significant number of fibrillar species are detected after 11 days (Figure 3).

Structural Perturbations Found in the *N*-Terminus of Fibrils Formed in the Presence of Anionic Phospholipid. An overlay of $^{13}C-^{13}C$ 2D spectra acquired on mature fibrils formed in the absence (blue) and presence of phospholipids (red) (Figure 4A) shows very good overall agreement, indicating that both fibrils have overall a similar fold. Further, similar morphology of the fibrils is observed with negative staining TEM, shown in Figure 4C,D. We next performed a complete study of the mature fibril samples, to site-specifically compare those incubated in the presence of lipids to those incubated in aqueous buffer. De novo chemical shift assignments of the backbone and side chains for the fibrils formed in the presence of phospholipid vesicles were obtained (Table S2, Supporting Information). A sequential backbone walk was conducted using multidimensional solid-state NMR experiments, as shown in Figure 5A for residues 83–86. A site-specific comparison of the chemical shifts demonstrates major and minor perturbations in the structure. The weighted average chemical shifts for the ^{13}CA and ^{15}NH, given by $|\Delta\delta|_{avg}$ (ppm) $= \{[\Delta\delta^2_{CA} + \Delta\delta^2_{NH}/(5/2)]/2\}^{1/2}$, is shown in Figure 5B as a function of residue number. These site-specific measurements demonstrate major perturbations ($|\Delta\delta|_{avg} \sim 0.2-4.0$ ppm) in the *N*-termini and minor perturbations ($|\Delta\delta|_{avg} \sim 0.2-0.7$ ppm) in residues located in the NAC domain. These results are in agreement with the overlaid expansions of the $^{13}C-^{13}C$ 2D correlation spectra shown in Figure 4B, with shifting of peaks that correspond to residues in the *N*-termini such as S42, T44, or V48.

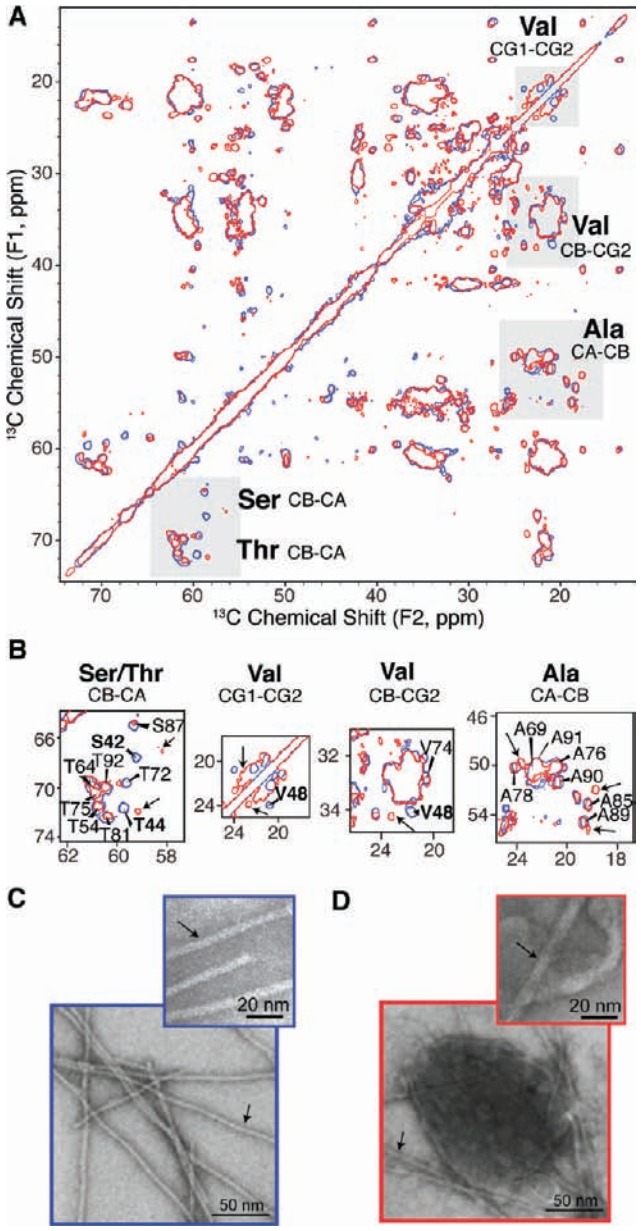

Figure 4. Comparison of AS fibrils formed in aqueous buffer and in the presence of phospholipids. (A) Overlay of $^{13}C-^{13}C$ 2D spectra (50 ms DARR mixing) of AS fibrils formed in aqueous buffer (blue) and in the presence of phospholipids (red). Spectra were collected at 750 MHz (^{1}H frequency). (B) Comparison of expanded regions marked in gray showing the shifting of some peaks in certain regions for the $^{13}C-^{13}C$ 2D spectra. Residues labeled in bold represent shifting, and new peaks are marked with arrows. Electron micrographs of AS fibrils formed (C) in aqueous buffer and (D) in the presence of phospholipids after 11 days of incubation. Arrows indicate AS fibrils in both images for comparison.

dx.doi.org/10.1021/ja209019s | J. Am. Chem. Soc. 2012, 134, 5090–5099

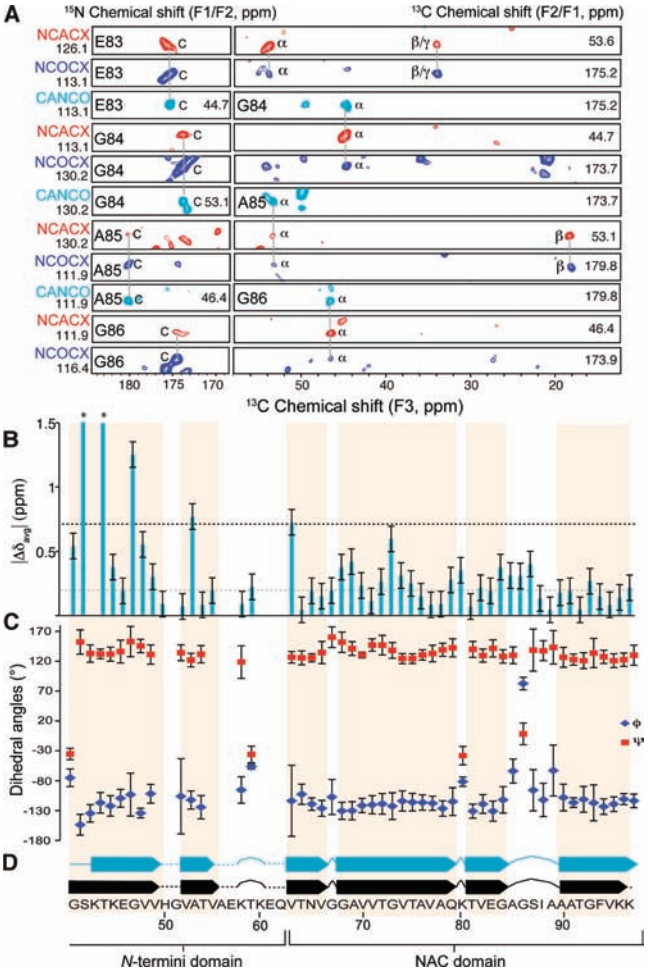

Figure 5. Secondary structure comparison between AS fibrils formed in aqueous buffer and in the presence of phospholipids. (a) Strip plot from the 3D NCACX, NCOCX, and CANCO spectra of U-^{13}C,^{15}N-labeled AS fibrils in the presence of phospholipids showing the sequential backbone connectivity for residues 83−86. (b) Weighted average chemical shift perturbations ($|\Delta\delta|_{avg}$) for the AS fibrils prepared in the presence of phospholipids versus the fibrils prepared in aqueous buffer. Error bars correspond to the chemical shift variations from one batch to another of the fibrils prepared in aquous buffer, as shown in ref 35. (c) TALOS+ predicted backbone dihedral angles φ and ψ as a function of residue number. Error bars are based on the 10 best TALOS+ database matches. (d) Representation of the TALOS +-predicted secondary structure of AS fibrils prepared in the presence of phospholipids (top) and in aqueous buffer (bottom) (arrows indicate β-strands; curved lines are turn or loop regions; dashed lines indicate no prediction).

Additionally, the presence of additional structured regions (indicated by arrows in Figure 4B), some with helical chemical shifts or residue types only present in the *N*-termini, supports the idea that the *N*-terminal domain anchors AS to the lipid bilayer and promotes the formation of β-sheet structures in registry throughout the NAC domain.[19] To test this hypothesis more robustly, we conducted 2D ^{1}H−^{13}C experiments with ^{1}H−^{1}H spin diffusion of the sample incubated for 0 days (state 1) and 1 day (state 2). Figure 6B shows representative planes for 256 ms mixing time; the protein to CH_2 lipids and protein to water cross-peaks can be clearly observed at the ^{1}H chemical shifts of ∼1.3 and 4.8 ppm, respectively. Cross-peak intensity for the ^{13}C chemical shifts from 50 to 70 ppm (corresponding primarily to protein signals; this was confirmed by DQ filtering experiments) was plotted as a function of mixing time (Figure 6A). The lipid acyl chain to AS correlations build up much more slowly than those from the water signals, consistent with an α-helical state (state 1) bound to the surface of the lipid bilayer. Signal patterns are consistent with those amino acid types most prominent in the *N*-terminal domain, and thus these results support the model in which AS is anchored on the surface of the lipid bilayer at the initial stages, as represented in Figure 7A. However, after 1 day of incubation, state 2 shows a similar buildup for the water and the lipid acyl curves (Figure 6C), suggesting the proximity of AS to the lipid acyl groups, in a manner expected when the protein is at least partially embedded in the lipid bilayer (Figure 7A).

In the absence of phospholipids, the initial state is less accessible to water, as shown by a comparison of the water-to-protein correlation trajectories for the two initial states trapped in the presence (Figure 6A,C) and absence of phospholipids (Figure S3A and S3B, Supporting Information). These differences further support the presence of different morphologies, as observed in the electron micrographs. On the basis of these results, we propose the formation of a hydrophobic core with β-sheet secondary structure in the absence of phospholipid vesicles (state 1, without phospholipids) that contrasts with the *N*-termini binding of AS with an α-helical secondary structure with the headgroups of phospholipids (state 1, with phospholipids), as represented in Figure 7. As AS (in the absence of phospholipids) converts to state 2, accessibility to water increases (Figure S3B, Supporting Information). This result is consistent with the stabilization of additional hydrophilic residues in this state 2, which is a well-defined sphere in the electron micrographs (Figures 3C and 7B).

In the presence of phospholipids, after further incubation (2 days) the AS is less strongly associated with the lipid acyl chains, as evidenced by a slower buildup curve for the lipid-to-protein correlation than the water-to-protein correlation (Figure 6D). Furthermore, at this point there are significant chemical shift changes observed in the ^{13}C−^{13}C 2D spectra. After 3 days, the electron micrographs show substantial perturbations in the phospholipid vesicles (Figure 3B), coinciding with the chemical shift pattern indicative of fibrils. Further comparison of the mature fibril buildup curves (Figure 6E) shows a similar trend for water and the lipids, in addition to a slower buildup than mature fibrils formed in aqueous media (Figure S3C, Supporting Information). We propose that this similarity in the buildup curves results from the fibrils being immersed in a network of vesicles with substantially perturbed morphology resulting from the fibril formation.

To further investigate the structural changes in the two final fibrillar states, an empirical prediction of the backbone torsion angles was obtained using the ^{13}C (CA, CB and CO) and ^{15}N chemical shift assignments and the TALOS+ program[49] (Figure 5C). TALOS+ predicts the secondary structure (Figure 5D) and demonstrates a similar repeated motif in the core of the fibrils as for those formed in aqueous buffer,[35] but with disruption of the longest β-strand from the *N*-termini, where we detect the largest perturbations in the chemical shifts.

Conformational Dynamics of Fibrils Formed in the Presence of Anionic Phospholipids. Our recent investigations of AS fibrils prepared in aqueous buffer[35] demonstrated the presence of conformational dynamics along the core of the fibrils and showed that the most rigid residues included the residues from T64 to K96. This region included residues 71

dx.doi.org/10.1021/ja209019s | J. Am. Chem. Soc. 2012, 134, 5090−5099

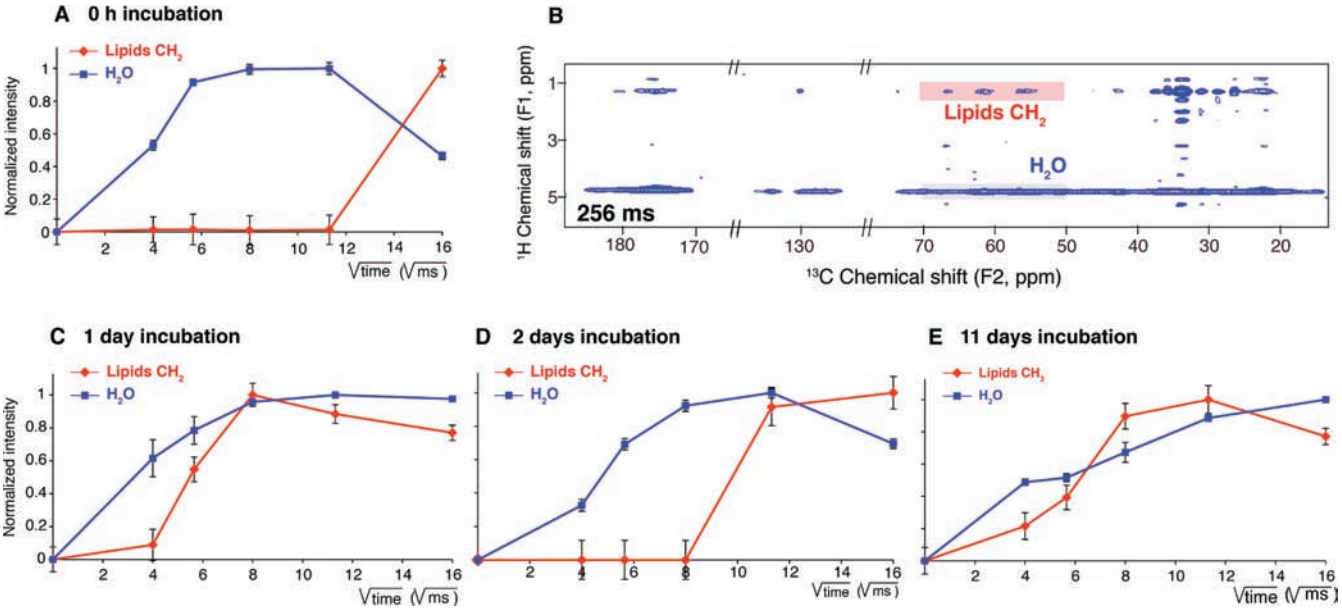

Figure 6. ^{1}H spin diffusion from lipid CH_2 chains and water to AS in the presence of phospholipids. ^{1}H spin diffusion buildup curves for lipid CH_2 chains (red) and water (blue) to AS for samples incubated with phospholipids for (A) 0, (C) 1, (D) 2, and (E) 11 days. (B) Selected 2D $^{1}H-^{13}C$ spectrum with a T_2 filter of 1.2 ms and $^{1}H-^{1}H$ spin difusion of 256 ms for samples incubated 11 days. Selected cross-peaks for the correlations between the lipid acyl chains and water to the protein are marked in red and blue, respectively. Data for the buildup curves were corrected for the ^{1}H T_1 relaxation. Error bars represent the error associated with the integration by NMRpipe of the 2D spectra.

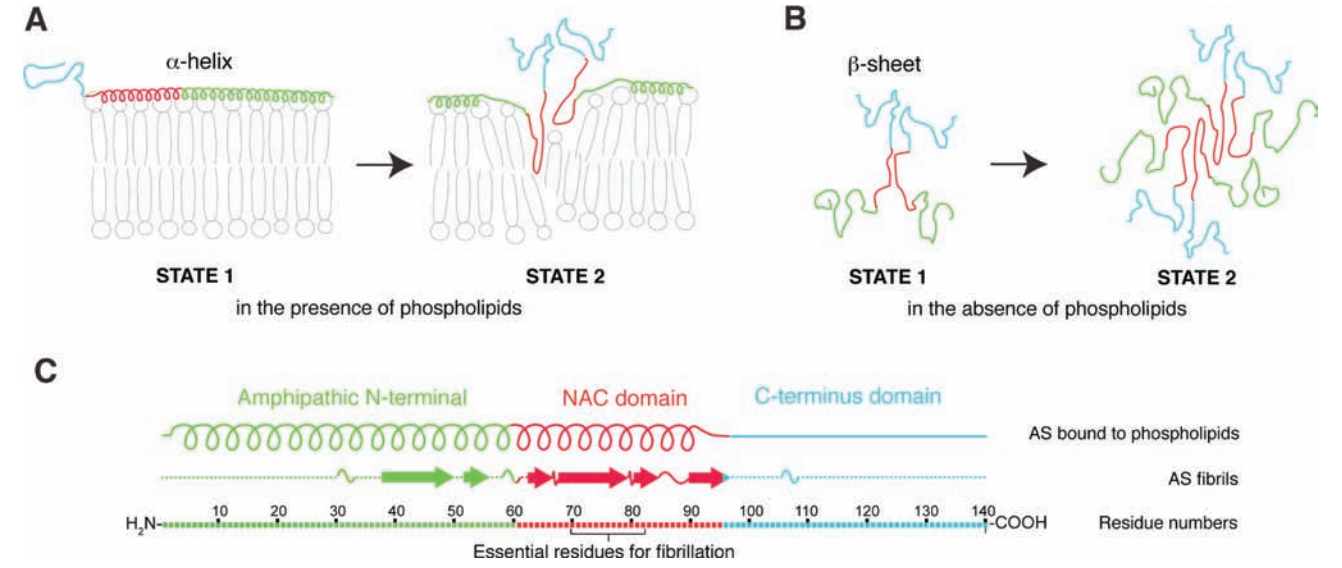

Figure 7. Schematic representation of the proposed mechanisms for AS fibril formation, (A) in the presence and (B) in the absence of phospholipids. (C) Schematic representation of the different domains of AS and predicted secondary structures of AS bound to phospholipids (top, ref 12) and AS fibrils prepared in aqueous buffer (bottom, ref 35). Arrows indicate β-strands; curved lines are turn or loop regions; dashed lines indicate no prediction. Essential residues for AS fibrillation (ref 50) are labeled in the residue numbers.

to 82 that were described by Giasson et al.[50] to be essential for AS fibril assembly. Considering the structural perturbations observed in the *N*-termini for this fibrillar state versus the fibrils formed in aqueous solution, we investigate further whether there were changes in the conformational dynamics versus the fibrils formed in aqueous buffer. In a site-specific qualitative manner, we confirmed no major conformational differences by performing a 3D CANCO experiment and normalizing the intensities to the strongest signal (A90CA-A90N-A89C). Almost all peaks between T64 and K96 had ~50% or greater intensity on this scale (Figure 8C). Therefore, the *N*-terminus of the fibrils formed in the presence of phospholipids is still a weaker signature than the residues located in the NAC domain, as previously shown for the fibrils formed in aqueous buffer. Additionally, these fibrils also present an overall similar predicted S^2 by TALOS+ (Figure 8B). To complement these results, direct polarization constant cross-peak correlation spectra (DP CTUC COSY)[35] were acquired on the fibrils formed in the presence and absence of anionic phospholipids (Figure 8A) to probe a similar structure for the dynamic regions. Overall, our results demonstrate high structural similarity between the dynamic regions of the fibrils, indicating only small perturbations (Figure 8A).

dx.doi.org/10.1021/ja209019s | J. Am. Chem. Soc. 2012, 134, 5090−5099

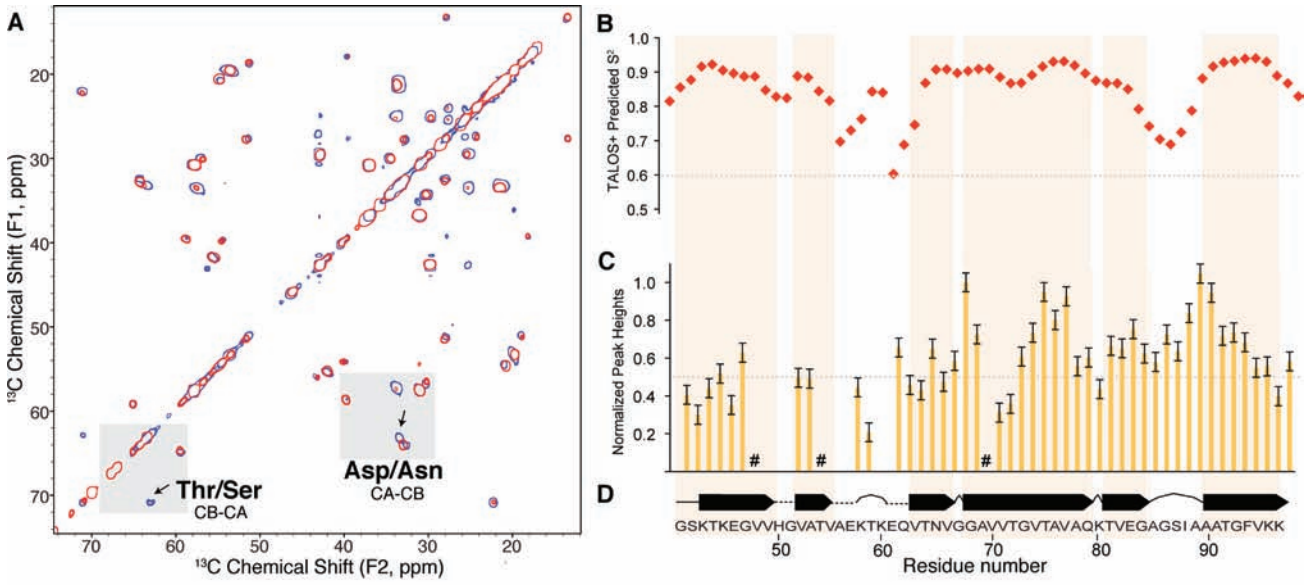

Figure 8. Conformational dynamics of AS fibrils formed in the presence of phospholipids. (A) Overlay of DP CTUC COSY spectra (4.5 ms) of AS fibrils formed in aqueous buffer (blue) and in the presence of phospholipids (red). Residues with perturbations are marked with arrows. (B) TALOS +-predicted order parameters S^2. (C) Relative peak heights from the cross-peak intensity of the 3D CANCO spectrum (numbered according to the carbonyl residue). Residues labeled as (#) correspond to residues with overlapped peaks in the CANCO experiment. Error bars correspond to the noise level. (D) Representation of the TALOS+-predicted secondary structure of AS fibrils prepared in the presence of phospholipids (arrows indicate β-strands; curved lines are turn or loop regions; dashed lines indicate no prediction).

Molecular Basis of α-Synuclein Fibril Formation in the Presence of Anionic Phospholipids. Our results demonstrate that the *N*-terminus and NAC domains of AS bind at the surface of the phospholipid vesicles with an α-helical conformation (state 1). After 1 day of incubation, we detected state 2 that interacts with the lipid acyl side chains of the phospholipids, which indicates embedding of AS in the phopholipid vesicles. After nucleation and formation of the initial β-sheet species, the sample matured into well-ordered fibrils, as shown by the chemical shift fingerprints shown in Figure 1. After 3 days of incubation, we observed the presence of well-resolved peaks that agreed with those of mature fibrils, such as V74, A76, or A78, that are within the residues demonstrated by Giasson et al. to be necessary for AS fibril assembly.[50] Additional peaks that did not change upon longer incubation times are also detected, such as A90 or A91, that are among the most rigid residues in the core of AS fibrils. All these residues are located in β-sheet regions of mature AS fibrils; this suggests that these are already well-packed by intermolecular contacts at this stage of fibril formation. As the fibrils mature, we detect changes in the observed correlations of some additional peaks, such as T59 or A85, that are located in loop regions of the mature fibrils. These changes could be attributed to a reduction of signal-to-noise, as T59 has weaker signal intensity in the mature fibrils than V74 or A78. However, A85 has a similar intensity as V74 in the mature fibrils. Therefore, this suggests that these contacts might be stabilized at a later stage of fibril formation.

■ CONCLUSIONS

In summary, we have captured different states on the pathway of AS structural transition from predominantly α-helical conformation to β-sheet fibrils, as indicated by the secondary chemical shifts and supported by the morphology changes in the electron micrographs. We have compared them to the fibrillation pathway in the absence of lipids. We have also demonstrated a similar fold and morphology between fibrils formed in the presence of phospholipid vesicles and in aqueous buffer, with major perturbations in the *N*-terminus and minor perturbations in the NAC domain. Our investigations demonstrate that AS binds at the surface of phospholipids with an α-helical secondary structure (state 1) and then converts to state 2 with a mostly β-sheet secondary structure and a close interaction with lipids. After 3 days of incubation, the nascent fibrils (sometimes also referred to as protofilaments) exhibit well-resolved peaks in the solid-state NMR spectra with key chemical shift signatures that agree with the mature fibrils. As fibrillation proceeds, further changes in chemical shifts corresponding to residues located in loop regions are observed, which indicates further stabilization of these regions at a later stage, likely due to quaternary assembly of protofilaments.

These results provide information at an atomic level on the pathway of conversion from the α-helical to β-sheet fibrillar states of AS in the presence of vesicles. By performing de novo chemical shift assignments of this fibrillar state, we have demonstrated major perturbations ($|\Delta\delta|_{avg} \sim 0.2-4.0$ ppm) in the *N*-terminus with partial disruption of the long β-strand located in the 40s and small perturbation ($|\Delta\delta|_{avg} \sim 0.2-0.7$ ppm) in residues located in the NAC domain. Despite these structural perturbations, conformational dynamics measurements of this fibrillar state show a much weaker signature for the β-strand located in the 40s, compared to the residues between T64 and K96. Similar results were observed for the fibrils formed in aqueous buffer.[35] Significantly, we detect the residues with stronger signature to already have the final structure, based on their chemical shifts, after only 3 days of fibrillation.

These investigations will serve as basis for further studies toward understanding how AS fibrils lead to the formation of

Lewy bodies,[51] the transmission of aggregates from neuron-to-neuron,[52] or the possible disruption of ionic homeostasis of neurons by fibrillar AS in disease.[23−25] Additionally, our results also demonstrate the feasibility and potential of solid-state NMR for the investigation of protein misfolding pathways and disease-associated amyloid fibril formation in the presence of phospholipids.

■ ASSOCIATED CONTENT

Supporting Information

^{1}H 1D spectra at different temperatures to confirm the phospholipid phase transition. Comparison of the ^{13}C−^{13}C 2D experiments and ^{1}H spin diffusion buildup curves for the samples incubated without phospholipids at different incubation times. Tables with the lipid-to-protein ratios at the different incubation times and chemical shift assignments. Chemical shift assignments have also been deposited to the BioMagResBank (BMRB) for release upon publication (BMRB entry number 17910). This material is available free of charge via the Internet at http://pubs.acs.org.

■ AUTHOR INFORMATION

Corresponding Author

rienstra@illinois.edu

Present Address

⊥Department of Physics, Oklahoma State University, Stillwater, Oklahoma 74074

Notes

The authors declare no competing financial interest.

■ ACKNOWLEDGMENTS

The work was supported by the National Institutes of Health (R01-GM073770) and utilized equipment procured with support of S10RR025037 from the National Center for Research Resources. G.C. was a Caja Madrid fellow and an Agusti Pedro Pons fellow. The authors thank Prof. Martin Gruebele, Dr. Ming Tang, and Dr. Jakob J. Lopez for helpful discussions and Lou A. Miller for advice and help with EM. Electron micrography was carried out in the Frederick Seitz Materials Research Laboratory Central Facilities, University of Illinois, which are partially supported by the U.S. Department of Energy under grants DE-FG02-07ER46453 and DE-FG02-07ER46471.

■ REFERENCES

(1) Spillantini, M. G.; Schmidt, M. L.; Lee, V. M. Y.; Trojanowski, J. Q.; Jakes, R.; Goedert, M. *Nature* **1997**, *388*, 839.

(2) Polymeropoulos, M. H.; Lavedan, C.; Leroy, E.; Ide, S. E.; Dehejia, A.; Dutra, A.; Pike, B.; Root, H.; Rubenstein, J.; Boyer, R.; Stenroos, E. S.; Chandrasekharappa, S.; Athanassiadou, A.; Papapetropoulos, T.; Johnson, W. G.; Lazzarini, A. M.; Duvoisin, R. C.; Di Iorio, G.; Golbe, L. I.; Nussbaum, R. L. *Science* **1997**, *276*, 2045.

(3) Kruger, R.; Kuhn, W.; Muller, T.; Woitalla, D.; Graeber, M.; Kosel, S.; Przuntek, H.; Epplen, J. T.; Schols, L.; Riess, O. *Nat. Genet.* **1998**, *18*, 106.

(4) Zarranz, J. J.; Alegre, J.; Gomez-Esteban, J. C.; Lezcano, E.; Ros, R.; Ampuero, I.; Vidal, L.; Hoenicka, J.; Rodriguez, O.; Atares, B.; Llorens, V.; Gomez Tortosa, E.; del Ser, T.; Munoz, D. G.; de Yebenes, J. G. *Ann. Neurol.* **2004**, *55*, 164.

(5) Chartier-Harlin, M. C.; Kachergus, J.; Roumier, C.; Mouroux, V.; Douay, X.; Lincoln, S.; Levecque, C.; Larvor, L.; Andrieux, J.; Hulihan, M.; Waucquier, N.; Defebvre, L.; Amouyel, P.; Farrer, M.; Destee, A. *Lancet* **2004**, *364*, 1167.

(6) Singleton, A. B.; Farrer, M.; Johnson, J.; Singleton, A.; Hague, S.; Kachergus, J.; Hulihan, M.; Peuralinna, T.; Dutra, A.; Nussbaum, R.; Lincoln, S.; Crawley, A.; Hanson, M.; Maraganore, D.; Adler, C.; Cookson, M. R.; Muenter, M.; Baptista, M.; Miller, D.; Blancato, J.; Hardy, J.; Gwinn-Hardy, K. *Science* **2003**, *302*, 841.

(7) Davidson, W. S.; Jonas, A.; Clayton, D. F.; George, J. M. *J. Biol. Chem.* **1998**, *273*, 9443.

(8) Perrin, R. J.; Woods, W. S.; Clayton, D. F.; George, J. M. *J. Biol. Chem.* **2000**, *275*, 34393.

(9) Eliezer, D.; Kutluay, E.; Bussell, R. Jr.; Browne, G. *J. Mol. Biol.* **2001**, *307*, 1061.

(10) Ulmer, T. S.; Bax, A.; Cole, N. B.; Nussbaum, R. *J. Biol. Chem.* **2005**, *280*, 9595.

(11) Bodner, C. R.; Dobson, C. M.; Bax, A. *J. Mol. Biol.* **2009**, *390*, 775.

(12) Jao, C. C.; Hedge, B. G.; Chen, J.; Haworth, I. S.; Langen, R. *Proc. Natl. Acad. Sci. U. S. A.* **2008**, *105*, 19666.

(13) Perrin, R. J.; Woods, W. S.; Clayton, D. F.; George, J. M. *J. Biol. Chem.* **2001**, *276*, 41958.

(14) Cole, N. B.; Murphy, D. D.; Grider, T.; Rueter, S.; Brasaemle, D.; Nussbaum, R. L. *J. Biol. Chem.* **2002**, *277*, 6344.

(15) Zhu, M.; Li, J.; Fink, A. L. *J. Biol. Chem.* **2003**, *278*, 40186.

(16) Necula, M.; Chirita, C. N.; Kuret, J. *J. Biol. Chem.* **2003**, *278*, 46674.

(17) Welch, K.; Yuan, J. Y. *Trends Neurosci.* **2003**, *26*, 517.

(18) Smith, D. P.; Tew, D. J.; Hill, A. F.; Bottomley, S. P.; Masters, C. L.; Barnhanm, K. J.; Cappai, R. *Biochemistry* **2008**, *47*, 1425.

(19) Bodner, C. R.; Maltsev, A. S.; Dobson, C. M.; Bax, A. *Biochemistry* **2010**, *49*, 862.

(20) Bartels, T.; Choi, J. G.; Selkoe, D. J. *Nature* **2011**, *477*, 107.

(21) Pandey, A. P.; Haque, F.; Rochet, J.-C.; Hovis, J. S. *Biophys. J.* **2009**, *96*, 540.

(22) Volles, M. J.; Lansbury, P. T. Jr. *Biochemistry* **2002**, *41*, 4595.

(23) Quist, A.; Doudevski, I.; Lin, H.; Azimova, R.; Ng, D.; Frangione, B.; Kagan, B.; Ghiso, J.; LaI, R. *Proc. Natl. Acad. Sci. U. S. A.* **2005**, *102*, 10427.

(24) Kim, H. Y.; Cho, M. K.; Kumar, A.; Maier, E.; Siebenhaar, C.; Bercker, S.; Fernandez, C. O.; Lashuel, H. A.; Benz, R.; Lange, A.; Zweckstetter, M. *J. Am. Chem. Soc.* **2009**, *131*, 17482.

(25) Lashuel, H. A.; Petre, B. M.; Wall, J.; Simon, M.; Nowak, R. J.; Walz, T.; Lansbury, P. T. Jr. *J. Mol. Biol.* **2002**, *322*, 1089.

(26) Lansing, J. C.; Hohwy, M.; Jaroniec, C. P.; Creemers, A. F.; Lugtenburg, J.; Herzfeld, J.; Griffin, R. G. *Biochemistry* **2002**, *41*, 431.

(27) Feng, X.; Verdegem, P. J.; Eden, M.; Sandstrom, D.; Lee, Y. K.; Bovee-Geurts, P. H.; de Grip, W. J.; Lugtenburg, J.; de Groot, H. J.; Levitt, M. H. *J. Biomol. NMR* **2000**, *16*, 1.

(28) Hornak, V.; Ahuja, S.; Eilers, M.; Goncalves, J. A.; Sheves, M.; Reeves, P. J.; Smith, S. O. *J. Mol. Biol.* **2010**, *396*, 510.

(29) Hu, K. N.; Yau, W. M.; Tycko, R. *J. Am. Chem. Soc.* **2010**, *132*, 24.

(30) Hu, K. N.; Tycko, R. *Biophys. Chem.* **2010**, *151*, 10.

(31) Chimon, S.; Shaibat, M. A.; Jones, C. R.; Calero, D. C.; Aizezi, B.; Ishii, Y. *Nat. Struct. Mol. Biol.* **2007**, *14*, 1157.

(32) Heise, H.; Hoyer, W.; Becker, S.; Andronesi, O. C.; Riedel, D.; Baldus, M. *Proc. Natl. Acad. Sci. U. S. A.* **2005**, *102*, 15871.

(33) Kloepper, K. D.; Zhou, D. H.; Li, Y.; Winter, K. A.; George, J. M.; Rienstra, C. M. *J. Biomol. NMR* **2007**, *39*, 197.

(34) Loquet, A.; Giller, K.; Becker, S.; Lange, A. *J. Am. Chem. Soc.* **2010**, *132*, 15164.

(35) Comellas, G.; Lemkau, L. R.; Nieuwkoop, A. J.; Kloepper, K. D.; Ladror, D. T.; Ebisu, R.; Woods, W. S.; Lipton, A. S.; George, J. M.; Rienstra, C. M. *J. Mol. Biol.* **2011**, *411*, 881.

(36) Gath, J.; Habenstein, B.; Bousset, L.; Melki, R.; Meier, B. H.; Bockmann, A. *Biomol. NMR Assign.* **2011**, DOI: 10.1007/s12104-011-9324-3.

(37) Kloepper, K. D.; Woods, W. S.; Winter, K. A.; George, J. M.; Rienstra, C. M. *Protein Expression Purif.* **2006**, *48*, 112.

(38) Hediger, S.; Meier, B. H.; Kurur, N. D.; Bodenhausen, G.; Ernst, R. R. *Chem. Phys. Lett.* **1994**, *223*, 283.

(39) Fung, B. M.; Khitrin, A. K.; Ermolaev, K. *J. Magn. Reson.* **2000**, *142*, 97.
(40) Comellas, G.; Lopez, J. J.; Nieuwkoop, A. J.; Lemkau, L. R.; Rienstra, C. M. *J. Magn. Reson.* **2011**, *209*, 131.
(41) Takegoshi, K.; Nakamura, S.; Terao, T. *Chem. Phys. Lett.* **2001**, *344*, 631.
(42) Morcombe, C. R.; Zilm, K. W. *J. Magn. Reson.* **2003**, *162*, 479.
(43) Van Geet, A. L. *Anal. Chem.* **1968**, *42*, 2227.
(44) Tang, M.; Sperling, L. J.; Berthold, D. A.; Nesbitt, A. E.; Gennis, R. B.; Rienstra, C. M. *J. Am. Chem. Soc.* **2011**, *133*, 4359.
(45) Goddard, T. D.; Kneller, D. G. *Sparky, version 3.106*; University of California: San Francisco.
(46) Jao, C. C.; Der-Sarkissian, A.; Chen, J.; Langen, R. *Proc. Natl. Acad. Sci. U. S. A.* **2004**, *101*, 8331.
(47) Georgieva, E. R.; Ramlall, T. F.; Borbat, P. P.; Freed, J. H.; Eliezer, D. *J. Biol. Chem.* **2010**, *285*, 28261.
(48) Havlin, R. H.; Tycko, R. *Proc. Natl. Acad. Sci. U. S. A.* **2005**, *102*, 3284.
(49) Cornilescu, G.; Delaglio, F.; Bax, A. *J. Biomol. NMR* **1999**, *13*, 289.
(50) Giasson, B. I.; Murray, I. V.; Trojanowski, J. Q.; Lee, V. M. Y. *J. Biol. Chem.* **2001**, *276*, 2380.
(51) Luk, K.; Song, C.; O'Brien, P.; Stieber, A.; Branch, J. R.; Brunden, K. R.; Trojanowski, J. Q.; Lee, V. M. Y. *Proc. Natl. Acad. Sci. U. S. A.* **2009**, *106*, 20051.
(52) Desplats, P.; Lee, H. J.; Bae, E. J.; Patrick, C.; Rockenstein, E.; Crews, L.; Spencer, B.; Masliah, E.; Lee, S. J. *Proc. Natl. Acad. Sci. U. S. A.* **2009**, *106*, 13010.